Modeling of Distributed Feedback Semiconductor Lasers with Axially-Varying Parameters

GOVIND P. AGRAWAL, SENIOR MEMBER, IEEE, AND ANDREW H. BOBECK, FELLOW, IEEE

Abstract—**We describe a numerical model that is capable of predicting important laser characteristics such as the threshold gain and the gain margin between the main and side modes for a distributed feedback (DFB) semiconductor laser of arbitrary complexity. The method consists of solving the coupled-mode equations with axially-varying parameters iteratively until the boundary conditions at the two facets are satisfied. We apply the numerical model to discuss two DFB laser structures. In the case of a multiple-phase-shift DFB laser our results show that such devices can have a more uniform axial distribution than that of a conventional quarter-wave-shifted DFB laser while maintaining sufficient gain margin between the main and side modes. In the case of a dual-pitch DFB laser we show that the incorporation of a slightly different grating period (~0.1 percent) over a small section can provide a gain margin that is comparable to that achieved in quarter-wave-shifted DFB lasers.**

I. Introduction

DISTRIBUTED feedback (DFB) semiconductor lasers have attracted considerable attention recently [1]–[5] because of their potential application in optical communication systems. Such lasers oscillate predominantly in a single longitudinal mode by virtue of a built-in index grating that provides dominant distributed feedback only in the vicinity of the Bragg wavelength determined by the grating period. The theoretical analysis of DFB lasers is generally based on the coupled-wave theory of Kogelnik and Shank [6]. For an axially-uniform DFB laser, the coupled-wave equations can be analytically solved to obtain an eigenvalue equation whose solution provides the threshold gains and the wavelengths of all the DFB modes [6]. However, if DFB lasers have intentional or unintentional variations in their parameters along the cavity length, it becomes necessary to solve the coupled-wave equations numerically in order to determine the DFB modes.

The objective of this paper is twofold. First, we discuss a numerical scheme that can determine the important device characteristics such as the threshold gain, the gain margin for side modes, and the differential quantum efficiency for a DFB laser with arbitrary axial variations. Second, we use this scheme to analyze two novel DFB structures. One structure is a generalization of the well-known quarter-wave-shifted DFB laser [2], i.e., in place of a single phase-shift region, it incorporates multiple phase-shift regions distributed over the cavity length. Such multiple phase-shift DFB lasers allow one to achieve a nearly-uniform axial intensity profile, thereby reducing the effect of spatial hole burning on the device performance. The other DFB structure is referred to as the dual-pitch DFB laser. In this device the grating period is made slightly different (~0.1 percent) over a section of the laser cavity. The numerical results show that for a relative section length of 0.25–0.35, the dual-pitch DFB laser can have a gain margin comparable to that of a quarter-wave-shifted DFB laser. Furthermore, when the laser cavity consists of two sections of equal lengths but different grating periods, the dual-pitch DFB laser acts as a dual-wavelength laser, i.e., the output from the two facets is dominated by two different modes oscillating at wavelengths whose difference is governed by the difference in the grating periods.

Manuscript received April 4, 1988; revised July 18, 1988.
The authors are with AT&T Bell Laboratories, Murray Hill, NJ 07974.
IEEE Log Number 8823791.

II. Coupled-Wave Equations

In DFB lasers, the use of a built-in grating leads to a periodic modulation of the refractive index of the optical mode propagating inside the active region (see Fig. 1). The index grating couples the forward and backward propagating waves through Bragg diffraction. In the coupled-wave analysis [6], the intracavity field is written as

$$E(z) = A(z)\exp(i\beta_0 z) + B(z)\exp(-i\beta_0 z) \quad (2.1)$$

where A and B are the amplitudes of the forward and backward propagating waves and β_0 is the Bragg wavenumber defined by [3]

$$\beta_0 = \frac{2\pi\bar{\mu}}{\lambda_B} = \frac{m\pi}{\Lambda}. \quad (2.2)$$

In (2.2), λ_B is the Bragg wavelength in vacuum, $\bar{\mu}$ is the effective mode index, Λ is the grating period, and m is the order of Bragg diffraction ($m = 1$ for a first-order grating). The use of (2.1) in the wave equation provides the coupled-wave equations:

$$\frac{dA}{dz} = (\alpha + i\delta)A + i\kappa B \quad (2.3)$$

$$\frac{dB}{dz} = -(\alpha + i\delta)B - i\kappa^* A \quad (2.4)$$

where α is the amplitude-gain coefficient given by

$$\alpha = (g - \alpha_{\text{int}})/2 \quad (2.5)$$

0018-9197/88/1200-2407$01.00 © 1988 IEEE

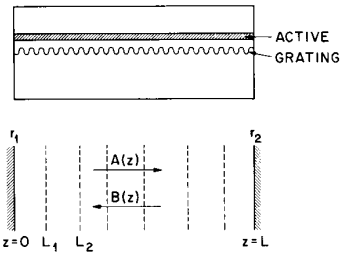

Fig. 1. Schematic illustration of a DFB semiconductor laser. The built-in grating couples the forward and backward waves propagating inside the active region, resulting in distributed feedback. The bottom portion shows the division of the cavity into subsections whose lengths depend on the specific DFB structure. A phase shift at the boundary of each subsection can also be incorporated in the numerical method used to model DFB lasers.

δ is a measure of the detuning of the laser mode from the Bragg wavelength

$$\delta = \beta - \beta_0 = 2\pi\bar{\mu}(1/\lambda - 1/\lambda_B) \qquad (2.6)$$

and κ is the coupling coefficient. The numerical value of κ depends on the fabrication details such as the layer thicknesses and the grating depth [3]. Typical values of κ are in the range 40–80 cm^{-1}. In (2.5), α_{int} accounts for the internal losses and g is the power gain. In the linear-gain approximation, g is related to the carrier density n inside the active region by [3]

$$g = \Gamma a(n - n_0) \qquad (2.7)$$

where Γ is the confinement factor, a is a proportionality constant (typically $a = 2 \times 10^{-16}$ cm^2), and n_0 is the carrier density required to overcome the intrinsic material loss ($n_0 = 1\text{–}1.5 \times 10^{18}$ cm^{-3}). It should be stressed that the index $\bar{\mu}$ is also a function of the carrier density n since in semiconductor lasers both the gain and the index are affected simultaneously by changes in the carrier density. More specifically,

$$\bar{\mu}(n) = \bar{\mu}(n_r) - \frac{\beta_c a \lambda}{4\pi}(n - n_r) \qquad (2.8)$$

where n_r is a reference carrier density. β_c is often referred to as the linewidth broadening parameter [7], [8] and has values typically in the range 3–8 for InGaAsP lasers.

The carrier density n in (2.7) depends on the pumping level and is obtained by solving [3]

$$\frac{dn}{dt} = \frac{I}{qV} - \frac{n}{\tau_c} - \frac{g(n)}{\hbar\omega}|E|^2 + D\nabla^2 n \qquad (2.9)$$

where I is the current flowing through the active region of volume V, τ_c is the carrier lifetime, $\hbar\omega$ is the photon energy at the lasing wavelength, q is the electron charge, and D is the diffusion coefficient. The solution of (2.9) is generally difficult to obtain if carrier diffusion is included through the last term. However, the main effect of diffusion is to wash out spatial holes burnt by interference of the counterpropagating forward and backward waves since their spacing $\lambda_B/2$ is much smaller than the diffusion length ($\sim$2–3 μm). Thus, to a good degree of approximation, we can ignore carrier diffusion by setting $D = 0$ provided we replace $|E|^2$ by the approximate form

$$|E(z)|^2 \simeq |A(z)|^2 + |B(z)|^2. \qquad (2.10)$$

The carrier density n is however still a function of z since the total intensity is not axially uniform in DFB lasers.

In the steady state ($dn/dt = 0$), (2.9) is readily solved with the result

$$n(z) = \frac{(I/I_0 + |E(z)|^2/P_s)\, n_0}{1 + |E(z)|^2/P_s} \qquad (2.11)$$

where $P_s = \hbar\omega/(\Gamma a \tau_c)$ is the saturation intensity (typically ~ 1 MW/cm^2) and $I_0 = qVn_0/\tau_c$ is the current required to achieve transparency. By using (2.5)–(2.8) we note that both α and δ are functions of z in the above-threshold regime because of local variations of the total optical intensity inside a DFB laser. This phenomenon is often referred to as spatial hole burning since an increase in the laser power results in a local reduction in the carrier density at places where the intracavity intensity is maximum. Near the laser threshold such that $|E(z)|^2 \ll P_s$, (2.11) becomes $n = (I/I_0)\, n_0$, and the carrier density n can be treated as constant along the laser length. Note, however, that n can still be z dependent if the current I is not the same all across the cavity length. This is, for example, the case for DFB lasers with segmented contacts.

The theoretical analysis of a DFB laser requires the solution of the coupled-wave equations (2.3) and (2.4) subject to the two boundary conditions at the laser facets

$$A(0) = r_1 B(0) \qquad B(L) = r_2 A(L) \qquad (2.12)$$

where the amplitude reflection coefficients

$$r_j = \sqrt{R_j}\exp(i\phi_j) \quad (j = 1, 2). \qquad (2.13)$$

In (2.13) R_j is the facet reflectivity and ϕ_j is the phase. The phases ϕ_1 and ϕ_2 take into account the phase shift occurring at the last incomplete period of the grating near the facets (see Fig. 1). In general, these phases can vary from device-to-device in a random manner.

The solution of (2.3) and (2.4) is relatively straightforward if the parameters α, δ, and κ are z independent, i.e., they do not vary along the cavity length. The use of boundary conditions (2.12) then results in an eigenvalue equation whose solution provides the threshold gain α and the detuning δ of various longitudinal modes supported by the DFB laser. Kogelnik and Shank [6] followed this approach for the specific case of nonreflecting facets ($R_1 = R_2 = 0$). Their method has been generalized to include the effect of facet reflections on the modes of a DFB laser [9], [10].

The assumption that α, δ, and κ are constant along the cavity length is not always justified. Equations (2.5)–(2.8) show that α and δ remain constant only if the carrier density n is axially uniform. Even if this is the case at threshold, gain saturation [11]–[14] in the above-threshold regime invariably leads to an axially-nonuniform carrier-density profile [(2.11)] because of spatial hole burning

[15]. As a result, both α and δ vary along the laser cavity. Such variations are continuous and depend on the axial intensity profile for the forward and backward propagating waves.

The parameters α, δ, and κ may not be constant along the cavity length even at threshold because of axial variations introduced intentionally to modify the device performance. Many specific structures have been studied [16]–[24] where at least one of the laser parameters is a function of z in (2.3) and (2.4). A particular structure that has attracted considerable attention recently [19]–[22] is the quarter-wave-shifted DFB laser in which a $\pi/2$ phase-shift is introduced in the middle of the laser cavity to force the laser to oscillate exactly at the Bragg wavelength [17]. Although this structure can be analyzed by considering two sections separately such that α, δ, and κ are constants in each section, a numerical approach becomes necessary when either the number of sections becomes large [24] or when the axial variations are truly continuous such as in the case of a chirped grating [18].

III. Numerical Procedure

We consider the most general case in which all three parameters α, δ, and κ can be z dependent in the coupled-wave equations (2.3) and (2.4). The objective is to find the mode gain $\bar{\alpha}$ and the mode detuning $\bar{\delta}$ defined by

$$\bar{\alpha} = \frac{1}{L}\int_0^L \alpha(z)\,dz \qquad \bar{\delta} = \frac{1}{L}\int_0^L \delta(z)\,dz \tag{3.1}$$

for various longitudinal modes of the laser cavity. The mode for which $\bar{\alpha}$ is smallest becomes the main mode since it reaches the threshold first. The mode with the second smallest value of $\bar{\alpha}$ plays the role of the dominant side mode. The main-mode threshold gain g_{th} and the gain margin $\Delta\alpha$ are defined by

$$g_{\text{th}} = 2\bar{\alpha}_{\text{th}} + \alpha_{\text{int}} \tag{3.2a}$$

$$\Delta\alpha = 2(\bar{\alpha}_{\text{SM}} - \bar{\alpha}_{\text{th}}) \tag{3.2b}$$

where $\bar{\alpha}_{\text{SM}}$ is the amplitude gain of the dominant side mode and $\bar{\alpha}_{\text{th}}$ is the amplitude gain of the main mode. The magnitude of $\Delta\alpha$ determines the extent to which the side mode is suppressed relative to the main mode [3].

We follow an iterative approach to obtain $\bar{\alpha}$ and $\bar{\delta}$ for several DFB modes. The starting values of A and B at $z = 0$ in (2.3) and (2.4) are chosen to satisfy the boundary condition $A(0) = r_1 B(0)$. The choice of $B(0)$ is arbitrary since it determines the intensity scale; we generally use $B(0) = 1$. An initial guess for $\bar{\alpha}$ and $\bar{\delta}$ is used to solve the coupled-wave equations and obtain the fields $A(L)$ and $B(L)$. These fields do not satisfy the boundary condition $B(L) = r_2 A(L)$ unless $\bar{\alpha}$ and $\bar{\delta}$ correspond to the actual values of the DFB mode. The mismatch

$$\epsilon = B(L) - r_2 A(L) \tag{3.3}$$

can however be used to estimate the corrections $\Delta\alpha$ and $\Delta\delta$ to the initial guess $\bar{\alpha}$ and $\bar{\delta}$. Noting that the change $\Delta\epsilon$ should be just large enough to cancel ϵ, we obtain $\Delta\epsilon = -\epsilon$, or

$$\frac{\partial\epsilon}{\partial\bar{\alpha}}\Delta\alpha + \frac{\partial\epsilon}{\partial\bar{\delta}}\Delta\delta = -\epsilon \tag{3.4}$$

where we used the fact that ϵ is a function of $\bar{\alpha}$ and $\bar{\delta}$. The real and imaginary parts of (3.4) provide two equations whose solution determines $\Delta\alpha$ and $\Delta\delta$. The process is repeated with the new values of $\bar{\alpha}$ and $\bar{\delta}$ until the boundary condition at $z = L$ is satisfied to the desired accuracy. In our simulations, the iteration process was assumed to converge when $|\epsilon| < 10^{-4}$.

The actual number of iterations required for convergence depends on the initial guess as well as on details of the laser structure. We have found it useful to take for the initial guess the values of $\bar{\alpha}$ and $\bar{\delta}$ expected for $\kappa = 0$. For the case of constant α and δ, the solution of (2.3) and (2.4) with the boundary condition (2.9) gives the threshold condition (similar to the case of a Fabry–Perot laser)

$$r_1 r_2 \exp\left[2(\bar{\alpha} + i\bar{\delta})L\right] = 1. \tag{3.5}$$

Equating the real and imaginary parts, we obtain

$$\bar{\alpha} = \frac{1}{4L}\ln\left(\frac{1}{R_1 R_2}\right) \tag{3.6}$$

$$\bar{\delta} = \frac{1}{2L}(2m\pi - \phi_1 - \phi_2) \tag{3.7}$$

where m is an integer. We have used (3.6) and (3.7) as an initial guess for $\bar{\alpha}$ and $\bar{\delta}$. The iteration procedure described above can refine the initial guess to an accuracy of about 10^{-4} in typically 3–5 interactions. Different DFB modes can be obtained by changing the value of m in (3.7). We vary m from -2 to 2 to obtain 5 DFB modes in the vicinity of the Bragg wavelength. The resulting values of $\bar{\alpha}$ and $\bar{\delta}$ for these DFB modes can be used to obtain the threshold gain and the location of the main mode as well as the gain margin $\Delta\alpha$ [see (3.2)].

The above scheme requires numerical integration of the coupled-mode equations (2.3) and (2.4) a large number of times. Although the well-known methods such as the Runge–Kutta algorithm [25] can be used for this purpose, we have found it better to use a matrix method [26] in which the cavity is divided into several subsections (see Fig. 1). In each subsection the parameters α, δ, and κ are treated as constants. Since (2.3) and (2.4) can then be solved analytically, the propagation through a subsection is carried out by using the prescription

$$\begin{pmatrix} A_{\text{out}} \\ B_{\text{out}} \end{pmatrix} = \begin{pmatrix} S_{AA} & S_{AB} \\ S_{BA} & S_{BB} \end{pmatrix} \begin{pmatrix} A_{\text{in}} \\ B_{\text{in}} \end{pmatrix} \tag{3.8}$$

where S is a 2×2 matrix with complex coefficients given by

$$S_{AA} = \frac{1}{1 - r^2}\left[\exp(iqh) - r^2 \exp(-iqh)\right] \tag{3.9}$$

$$S_{BB} = \frac{1}{1 - r^2}\left[\exp(-iqh) - r^2 \exp(iqh)\right] \quad (3.10)$$

$$S_{BA} = -S_{AB} = \frac{r}{1 - r^2}\left[\exp(iqh) - \exp(-iqh)\right]. \quad (3.11)$$

In (3.9)–(3.11), h is the subsection length,

$$q = \pm i\left[(\alpha + i\delta)^2 + \kappa^2\right]^{1/2} \quad (3.12)$$

and

$$r = \frac{q + i(\alpha + i\delta)}{\kappa} = \frac{-\kappa}{q - i(\alpha + i\delta)}. \quad (3.13)$$

The parameter r can be interpreted as the effective reflection coefficient of the grating [3]. The sign in (3.12) is chosen such that $|r(q)| < 1$. The forward and backward propagating fields can be propagated across the entire cavity length through successive use of (3.8) in going from one subsection to next. The matrix method is considerably faster compared with other direct integration methods (implicit or explicit) for a given accuracy.

In some DFB laser structures such as a quarter-wave-shifted DFB laser, the intracavity field experiences a phase shift at certain locations along the cavity length. The algorithm described above can easily be generalized to include the additional built-in phase shifts. While dividing the cavity into subsections, the subsection boundaries are forced to coincide with the phase-shift locations. The phase shift at the subsection boundary is included by using

$$\begin{pmatrix} A_{\text{out}} \\ B_{\text{out}} \end{pmatrix} = \begin{pmatrix} \exp(i\phi_{\text{sh}}) & 0 \\ 0 & \exp(-i\phi_{\text{sh}}) \end{pmatrix} \begin{pmatrix} A_{\text{in}} \\ B_{\text{in}} \end{pmatrix} \quad (3.14)$$

where ϕ_{sh} is the amount of phase shift. In the matrix method, it amounts to multiplying the field components by a diagonal matrix, a procedure readily implemented.

The numerical algorithm was tested on two specific DFB laser structures for which the threshold gain $\bar{\alpha}$ and the mode detuning $\bar{\delta}$ can also be obtained using the conventional eigenvalue method based on the analytic solution of the coupled-wave equations. For the conventional DFB laser, the whole cavity acts as a single section. For the quarter-wave-shifted DFB lasers, the laser cavity is divided into two subsections with $\phi_{\text{sh}} = \pi/2$ at $z = L/2$. In both cases the results based on the numerical approach described here agreed with those obtained using the eigenvalue method with a relative accuracy of better than 10^{-4}. It should be noted that the present method automatically provides the axial intensity distribution of the forward and propagating waves for each mode. This is useful to estimate the extent of spatial hole burning. At the same time it can be used to calculate the differential quantum efficiency of the light emitted from the two facets. More specifically,

$$\eta_1 = \eta_d \frac{P_1}{P_1 + P_2} \qquad \eta_2 = \eta_d \frac{P_2}{P_1 + P_2} \quad (3.15)$$

where

$$P_1 = C(1 - R_1)\left|B(0)\right|^2 \qquad P_2 = C(1 - R_2)\left|A(L)\right|^2 \quad (3.16)$$

are the powers emitted from the facets located at $z = 0$ and $z = L$, respectively, C is a normalization constant, and

$$\eta_d = \eta_i \frac{2\bar{\alpha}_{\text{th}}}{2\bar{\alpha}_{\text{th}} + \alpha_{\text{int}}} \quad (3.17)$$

is the total differential quantum efficiency. In (3.17), η_i is the internal quantum efficiency, $\bar{\alpha}_{\text{th}}$ is the threshold gain of the main mode, and α_{int} is the total internal loss resulting from the phenomena such as free-carrier absorption and interface scattering.

IV. Results

In this section we apply the general numerical method discussed in Section III to two DFB laser structures of interest. Although the method can be used in the above-threshold regime by including gain saturation, we focus our attention to the near-threshold regime in which the output power is far below the saturation level (typically 3–5 mW). The objective is to determine how the laser characteristics such as the threshold gain $\bar{\alpha}_{\text{th}}$ and the gain margin $\Delta\alpha$ depend on the structural changes that lead to axial variations of the DFB laser parameters. The two structures discussed in detail are 1) a multiple-phase-shift DFB laser and 2) a dual-pitch DFB laser.

A. Multiple-Phase-Shift DFB Lasers

The multiple-phase-shift DFB laser [23], [24] is a generalization of the quarter-wave-shifted DFB laser [22] in which a single phase shift of $\pi/2$ is incorporated in the middle of the laser cavity. The motivation behind considering multiple phase-shift regions is as follows. It is well known [15] that in quarter-wave-shifted DFB lasers, the total intracavity intensity peaks in the middle of the cavity near the phase-shift region. As a consequence, gain saturation in the above-threshold regime can lead to significant local changes in the carrier density which in turn changes the refractive index locally through the relation (2.8). This phenomenon of spatial hole burning can affect the laser characteristics dramatically [15]. In particular, it reduces the gain margin $\Delta\alpha$ with an increase in the output power, an undesirable feature. The problem of spatial hole burning is less severe if the axial intensity profile is nearly uniform across the cavity length. We have found that the use of multiple phase shift regions can make the intensity profile more uniform than that of conventional quarter-wave-shifted DFB lasers.

Fig. 2 shows the threshold gain g_{th} of the main mode and the gain margin $\Delta\alpha$ as a function of the phase shift ϕ_{sh} for the cases of $N_{\text{sh}} = 1$–3, where N_{sh} is the number of phase-shift locations. For definiteness, we have assumed that the phase shift locations are equispaced across the cavity length and that the same phase shift occurs at

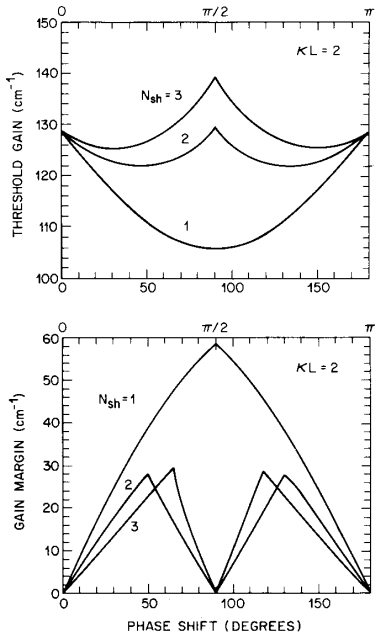

Fig. 2. Variation of the threshold gain g_{th} and the gain margin $\Delta\alpha$ with the phase shift ϕ_{sh} for multiple phase-shift DFB lasers. The case $N_{sh} = 1$ with $\phi_{sh} = \pi/2$ corresponds to the conventional quarter-wave-shifted DFB laser.

each location. Thus for $N_{sh} = 3$, a phase shift of ϕ_{sh} occurs at $z = L/4$, $L/2$, and $3L/4$. The coupling coefficient κ was chosen such that $\kappa L = 2$. For $L = 250$ μm, a typical value of the cavity length, this corresponds to $\kappa = 80$ cm^{-1}. The internal loss was taken to be $\alpha_{int} = 50$ cm^{-1}. In order to avoid complications resulting from the grating phases ϕ_1 and ϕ_2 at the facets (which may vary from device to device), we have taken $R_1 = R_2 = 0$. The effect of residual facet reflections is to replace each curve in Fig. 2 by a band resulting from variations in the phases ϕ_1 and ϕ_2. The qualitative behavior however remains unchanged for facet reflectivities of 1 percent or less. The main conclusion drawn from Fig. 1 is that multiple phase shifts can provide significant gain margin in the range 20–30 cm^{-1} if the amount of phase shift ϕ_{sh} is optimized. Although the gain margin $\Delta\alpha$ is roughly reduced by a factor of two compared with conventional quarter-wave-shifted DFB lasers ($N_{sh} = 1$ and $\phi_{sh} = \pi/2$), the DFB side modes are still suppressed by 30 dB or more as long as $\Delta\alpha > 8$–10 cm^{-1} [27], [28]. The threshold gain is also generally increased for $N_{sh} > 1$. However, at the optimum values of the phase shift, the increase is about 20 percent, which would not increase the threshold current significantly.

As discussed above, the motivation behind the multiple phase-shift regions is to achieve nearly-uniform axial intensity profiles. Fig. 3 compares the main-mode intensity profiles for $N_{sh} = 1$–3 with the optimum value of the phase shift for each N_{sh}. More specifically, the total intensity $P(z) = |A(z)|^2 + |B(z)|^2$ is plotted, where $A(z)$ and

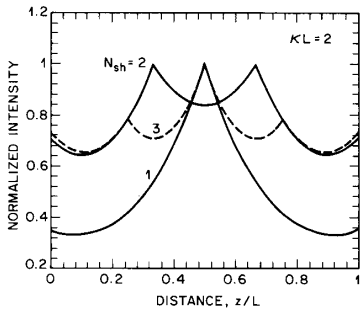

Fig. 3. Axial distribution of the main-mode intensity for $N_{sh} = 1$–3. For each value of N_{sh}, the phase shift ϕ_{sh} is chosen to be the one for which $\Delta\alpha$ is largest in Fig. 2.

$B(z)$ are obtained by solving the coupled-wave equations (2.3) and (2.4). Note that the peaks in $P(z)$ occur at places where the phase shift was introduced. The important point to note is that the use of multiple phase shifts reduces considerably the range over which $P(z)$ varies inside the laser cavity. As a result, spatial hole burning is less of a problem, and the performance of such lasers is expected to be less dependent on the operating power. Note that even two phase-shift regions are enough to take advantage of the concept of the multiple phase shifts.

The relatively flat intensity distribution in the case of multiple-phase-shift DFB lasers in a consequence of the boundary conditions imposed on the electric field at the location of the phase shifts. Near each phase discontinuity the field must decay exponentially while, at the same time, peaking at the discontinuity itself. As the phase discontinuities come closer, the decaying field near one discontinuity is forced to start rising before it has a chance to decay considerably. Note that the situation is different from that considered in [23] where identical phase-shifted (single $\pi/2$ shift) lasers are coupled in series. There, the axial variation of the field intensity remains unchanged for a given value of the coupling coefficient.

B. Dual-Pitch DFB Lasers

In a dual-pitch DFB laser, the laser consists of two sections of slightly different grating periods. Let us assume that in a section of length L_1 the grating period is $\Lambda + \Delta\Lambda$ while the remaining section of length $L - L_1$ has the period Λ. As seen in (2.2), for a first-order grating the Bragg wavelength is related to the grating period by the simple relation

$$\lambda_B = 2\bar{\mu}\Lambda \tag{4.1}$$

where $\bar{\mu}$ is the effective index. Because of different grating periods the two sections have different Bragg wavelengths. The motivation behind the dual-pitch DFB laser is as follows. A conventional single-pitch DFB laser with nonreflecting facets ($R_1 = R_2 = 0$) has two modes with the same threshold gain located at the edge of the stopband [6]. A dual-pitch DFB laser can be viewed as two coupled conventional DFB lasers whose stopbands are shifted with respect to each other by $\Delta\lambda_B = 2\bar{\mu}\Delta\Lambda$. If the

shift $\Delta\lambda_B$ is suitably chosen such that the left-hand side edge of one stopband coincides with the right-hand side edge of the other stopband, this particular mode will be favored in both sections and will have the lowest threshold gain. The other modes will be discriminated since they are not supported simultaneously by both sections. In this respect, a dual-pitch DFB laser selects a single longitudinal mode in a manner similar to that of a coupled-cavity laser [3]. Note that a relatively small change $\Delta\Lambda/\Lambda \simeq 1 \times 10^{-3}$ is required since a relative change of 0.1 percent in Λ corresponds to $\Delta\lambda_B \simeq 1.5$ nm (for $\lambda_B \simeq 1.55$ μm), a typical value for the width of the stopband.

For the numerical results, we have again selected the parameter values used in Figs. 2 and 3. More specifically, we take $L = 250$ μm, $\kappa L = 2$, $\alpha_{int} = 50$ cm^{-1}, and $R_1 = R_2 = 0$. Fig. 4 shows the gain margin $\Delta\alpha$ and the main-mode threshold gain g_{th} as a function of the section length L_1 for several values of $\Delta\Lambda/\Lambda$. The parameter L_1 is varied only in the range 0–$L/2$ because of the inherent symmetry of the device about $z = L/2$. In particular, note that a dual-pitch device with two sections of equal lengths has $\Delta\alpha = 0$. However, considerable gain margin can be realized if L_1/L is chosen to be in the range 0.25–0.35. The amount of gain margin $\Delta\alpha$ depends on the value of $\Delta\Lambda/\Lambda$; $\Delta\alpha \simeq 30$ cm^{-1} can be obtained for $\Delta\Lambda/\Lambda \simeq 0.1$ percent. Even higher values of $\Delta\alpha$ are possible by increasing $\Delta\Lambda$. The kinks seen in Fig. 4 for $\Delta\Lambda/\Lambda \geq 1.5 \times 10^{-3}$ correspond to mode jumps. The origin of these mode jumps can be understood by noting that for such large values of $\Delta\Lambda$, the stopbands of the two sections are separated by more than the widths of the individual stopbands. Thus, depending on the section lengths, the laser oscillates in the vicinity of one stopband or the other. The central region between the two kinks correspond to the case in which two sections cooperate with each other.

To understand the mode of operation of a dual-pitch DFB laser, it is instructive to look at the axial distribution of the mode intensity inside the laser cavity. Fig. 5 shows the main-mode axial distributions of the forward wave $|A(z)|^2$, the backward wave $|B(z)|^2$, and the sum $|A(z)|^2 + |B(z)|^2$ for the specific case of $L_1/L = 1/2$ and $\Delta\Lambda/\Lambda = 1.5 \times 10^{-3}$. Fig. 6 shows the same distributions for the side mode. A comparison of Figs. 5 and 6 shows that the axial distributions of the main and side modes are the mirror image of each other. This behavior can be understood by noting that for $L_1 = L/2$, the device has two sections of equal length with zero gain margin (Fig. 4), i.e., the main and side modes reach threshold simultaneously. However, since the two sections have different Bragg wavelengths (because of slightly different grating periods), the main mode of one section becomes the side mode of the other section. In effect, such a laser acts as a dual-wavelength laser emitting its light predominantly at one wavelength from one facet and at a different wavelength from the other facet. Figs. 5 and 6 show that the power ratio at the two wavelengths from each facet is about 6:1. Although this value of mode-suppression ratio is not large enough for single-frequency applications, such

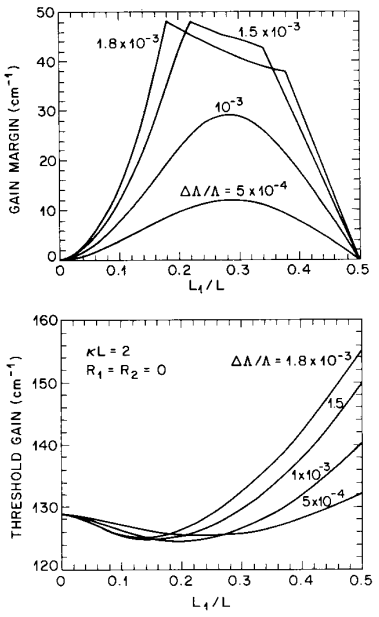

Fig. 4. Variation of the gain margin $\Delta\alpha$ and the threshold gain g_{th} with the section length L_1 for a dual-pitch DFB laser. Different curves correspond to different values of the relative pitch increase $\Delta\Lambda/\Lambda$ over the section of length L_1.

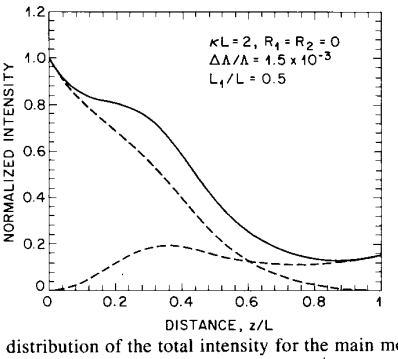

Fig. 5. Axial distribution of the total intensity for the main mode of dual-pitch DFB lasers of equal section lengths ($L_1 = L/2$) and $\Delta\Lambda/\Lambda = 1.5 \times 10^{-3}$. Other device parameters are identical to those of Fig. 4. Dashed curves show the axial distribution of the forward and backward propagating waves.

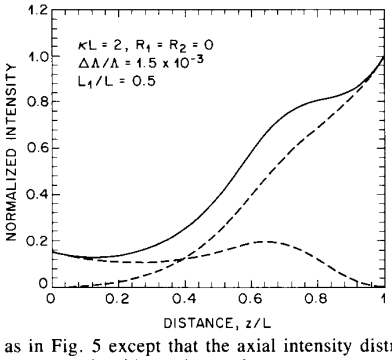

Fig. 6. Same as in Fig. 5 except that the axial intensity distributions for the side mode are shown.

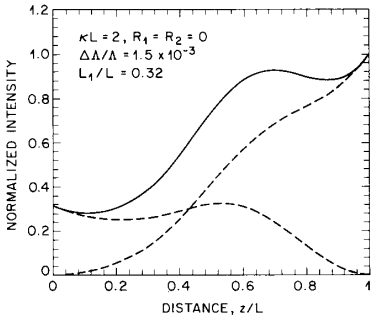

Fig. 7. Same as in Fig. 5 except that the axial intensity distributions are shown for $L_1/L = 0.32$.

a dual-wavelength laser may be useful for many other applications. An important feature of such lasers is that the wavelength difference $\Delta\lambda_B$ can be controlled by adjusting the difference $\Delta\Lambda$ in the grating period of two sections.

When the two sections are of different lengths, the large values of $\Delta\alpha$ in Fig. 4 imply that the wavelength associated with the longer section will dominate the device behavior. Fig. 7 shows the axial distribution of the main mode for $L_1/L = 0.32$ and $\Delta\Lambda/\Lambda = 1.5 \times 10^{-3}$. The side-mode intensity on the scale of Fig. 7 nearly coincides with the x axis because of the large gain margin between the two modes ($\Delta\alpha = 42\ \text{cm}^{-1}$ from Fig. 4). Note that it is advantageous to extract the power from the longer-section side because that section plays a dominant role. The purpose of the smaller section is to provide a gain margin between the main and side modes. The extent of gain margin depends on the period difference $\Delta\Lambda$ as seen in Fig. 4.

V. Conclusion

In this paper we have described a numerical procedure that is capable of predicting important laser characteristics such as the threshold gain and the gain margin for a DFB semiconductor laser of arbitrary complexity. We have applied the method to model two DFB laser structures. In the case of a multiple-phase-shift DFB laser, our results show that such devices can have a more uniform axial intensity distribution than that of a quarter-wave-shifted (single-shift) DFB laser while maintaining sufficient gain margin between the main and side modes. Such devices are likely to be more stable in the above-threshold regime since spatial hole burning plays a less important role. In the case of a dual-pitch DFB laser, we show that the incorporation of a slightly different grating period over a section with a relative length of 0.25–0.35 can provide a gain margin that is comparable to that achieved in quarter-wave-shifted DFB laser. Such lasers therefore represent an alternative to the quarter-wave-shifted DFB laser. At the same time, if the lengths of the two sections are made nearly equal, a dual-pitch DFB laser acts as two lasers in one housing, i.e., the output is dominated at a different wavelength for each facet. We believe that the numerical method presented here is versatile and can be used to test many different ideas. Although in this paper we did not include the gain saturation, this numerical method is currently being used to investigate spatial hole burning effects in the above-threshold regime.

References

[1] Y. Itaya, H. Saito, G. Motosugi, and Y. Tohmori, "Low threshold current GaInAsP/InP DFB lasers," *IEEE J. Quantum Electron.*, vol. QE-23, pp. 828–834, 1987.

[2] S. Akiba, M. Usami, and K. Utaka, "1.5-μm $\lambda/4$-shifted InGaAsP/InP DFB lasers," *J. Lightwave Technol.*, vol. LT-5, pp. 1564–1573, 1987.

[3] G. P. Agrawal and N. K. Dutta, *Long-Wavelength Semiconductor Lasers*. New York: Van Nostrand, 1986, ch. 7.

[4] Y. Suematsu, K. Kishino, S. Arai, and F. Koyama, "Dynamic single-mode semiconductor lasers with a distributed reflector," in *Semiconductors and Semimetals*, vol. 22B, W. T. Tsang, Ed. Orlando, FL: Academic, 1985, ch. 4.

[5] G. P. Agrawal, "Single-longitudinal-mode semiconductor lasers," in *Progress in Optics*, vol. 26, E. Wolf, Ed. Amsterdam, The Netherlands: North-Holland, 1988, ch. 3.

[6] H. Kogelnik and C. V. Shank, "Coupled-wave theory of distributed feedback lasers," *J. Appl. Phys.*, vol. 43, pp. 2327–2335, 1972.

[7] C. H. Henry, "Theory of the linewidth of semiconductor lasers," *IEEE J. Quantum Electron.*, vol. QE-18, pp. 259–264, 1982.

[8] M. Osiński and J. Buus, "Linewidth broadening factor in semiconductor lasers—An overview," *IEEE J. Quantum Electron.*, vol. QE-23, pp. 9–29, 1987.

[9] W. Streifer, R. D. Burnham, and D. R. Scifres, "Effect of external reflectors on longitudinal modes of distributed feedback lasers," *IEEE J. Quantum Electron.*, vol. QE-11, pp. 154–156, 1975.

[10] R. F. Kazarinov and C. H. Henry, "Second-order distributed feedback lasers with mode selection provided by first-order radiation losses," *IEEE J. Quantum Electron.*, vol. QE-21, pp. 144–150, 1985.

[11] K. O. Hill and A. Watanabe, "Envelope gain saturation in distributed-feedback lasers," *Appl. Opt.*, vol. 14, pp. 950–961, 1975.

[12] H. A. Haus, "Gain saturation in distributed feedback lasers," *Appl. Opt.*, vol. 14, pp. 2650–2652, 1975.

[13] K. O. Hill and R. T. MacDonald, "Gain saturation in DFB lasers with end reflectors," *IEEE J. Quantum Electron.*, vol. QE-12, pp. 716–721, 1976.

[14] P. Szczepański, "Approximate analysis of gain saturation of a distributed feedback laser with end reflectors," *IEEE J. Quantum Electron.*, vol. QE-22, pp. 517–519, 1986.

[15] H. Soda, Y. Kotaki, H. Sudo, H. Ishikawa, S. Yamakoshi, and H. Imai, "Stability in single longitudinal mode operation in GaInAsP/InP phase-adjusted DFB lasers," *IEEE J. Quantum Electron.*, vol. QE-23, pp. 804–814, 1987.

[16] R. Shubert, "Theory of optical-waveguide distributed lasers with nonuniform gain and coupling," *J. Appl. Phys.*, vol. 45, pp. 209–215, 1974.

[17] H. A. Haus and C. V. Shank, "Antisymmetric taper of distributed feedback lasers," *IEEE J. Quantum Electron.*, vol. QE-12, pp. 532–539, 1976.

[18] A. Suzuki and K. Tada, "Theory and experiment on distributed feedback lasers with chirped grating," *Proc. SPIE*, vol. 239, pp. 10–18, 1980.

[19] K. Tada, Y. Nakano, and A. Ushirokawa, "Proposal of a distributed feedback laser with nonuniform stripe width for complete single-mode oscillation," *Electron. Lett.*, vol. 20, pp. 82–84, 1984.

[20] N. Eda, K. Furuya, F. Koyama, and Y. Suematsu, "Axial mode selectivity in active distributed reflector for dynamic-single-mode lasers," *J. Lightwave Technol.*, vol. LT-3, pp. 400–407, 1985.

[21] S. L. McCall and P. M. Platzman, "An optimized $\pi/2$ distributed feedback laser," *IEEE J. Quantum Electron.*, vol. QE-21, pp. 1899–1904, 1985.

[22] K. Utaka, S. Akiba, K. Sakai, and Y. Matsushima, "$\lambda/4$-shifted InGaAsP/InP DFB lasers," *IEEE J. Quantum Electron.*, vol. QE-22, pp. 1042–1051, 1986.

[23] T. Kimura and A. Sugimura, "Linewidth reduction by coupled phase-shift distributed-feedback lasers," *Electron. Lett.*, vol. 23, pp. 1014–1015, Sept. 1987.

[24] G. P. Agrawal, J. E. Geusic, and P. J. Anthony, "Distributed feedback lasers with multiple phase-shift regions," *Appl. Phys. Lett.*, vol. 53, pp. 178–179, July 1988.

[25] W. H. Press, B. P. Flannery, S. A. Teukolsky, and W. T. Vetterling, *Numerical Recipes*. New York: Cambridge Univ., 1986, ch. 15.
[26] M. Yamada and K. Sakuda, "Analysis of almost periodic distributed feedback slab waveguides via a fundamental matrix approach," *Appl. Opt.*, vol. 26, pp. 3474-3478, 1987.
[27] G. Motosugi, Y. Yoshikuni, and T. Ikegami, "Single-longitudinal-mode condition for DFB lasers," *Electron. Lett.*, vol. 21, pp. 352-353, 1985.
[28] T. Matsuoka, Y. Yoshikuni, and G. Motosugi, "Dependence of single-longitudinal-mode probability on DFB laser facet structure," *Electron. Lett.*, vol. 21, pp. 1151-1152, 1985.

Govind P. Agrawal (M'83-SM'86), for a photograph and biography, see p. 142 of the February 1988 issue of this JOURNAL.

Andrew H. Bobeck (S'48-A'50-M'55-F'71) was born in Tower Hill, PA on October 1, 1926. He received the M.S.E.E. degree from Purdue University, West Lafayette, IN, in 1949 and an Honorary Doctor of Engineering in 1972.

Since 1949 he has been a member of the staff at AT&T Bell Laboratories, Murray Hill, NC, where he specialized in the development of magnetic components. More recently he began research and development of photonic devices. His contributions included the design of the first solid-state driven core memory, the invention of the twistor memory and co-invention of the magnetic bubble memory concept. He has been granted 121 U.S. patents.

Mr. Bobeck is a member of the National Academy of Engineering. His previous awards include the Valdemar Poulsen Gold Medal of the Danish Academy of Technical Sciences.